

17
—
N63-10204 Code 1

NASA TN D-1097

NASA TN D-1097



TECHNICAL NOTE

D-1097

SCANNING MECHANISM FOR A SATELLITE BORNE X-RAY SPECTROMETER

Gerald L. Hempfling

Goddard Space Flight Center
Greenbelt, Maryland

NATIONAL AERONAUTICS AND SPACE ADMINISTRATION
WASHINGTON

November 1962



SCANNING MECHANISM FOR A SATELLITE BORNE X-RAY SPECTROMETER

by

GERALD L. HEMPFLING
Goddard Space Flight Center

SUMMARY

One experiment aboard the Orbiting Solar Observatory I satellite (1962 ζ) employs an X-ray spectrometer. Three distinct mechanisms were designed to perform this instrument's scanning function, i.e., moving the detector along the focal curve; the mechanism which proved most satisfactory was to be used in the satellite. The design and testing of one such mechanism is documented here. This device also maintains the detector perpendicular to the radiation beam incident from the grating, as the detector moves along the focal curve. It was later decided that there was no certain advantage in maintaining this perpendicularity of the detector. Hence, one of the simpler mechanisms lacking the incidence correction feature was selected for use in the satellite. The information presented in this report should be useful in the future designing of similar devices, particularly when the detector is required to remain perpendicular to the incident rays.



CONTENTS

Summary	i
INTRODUCTION	1
DESIGN SPECIFICATIONS	2
DESIGN, FABRICATION, AND INSPECTION	4
TESTING	5
CONCLUSION AND RECOMMENDATIONS	9
Appendix A—Determination of the Pointing Accuracy	10

SCANNING MECHANISM FOR A SATELLITE BORNE X-RAY SPECTROMETER

by
GERALD L. HEMPFLING
Goddard Space Flight Center

INTRODUCTION

The Orbiting Solar Observatory I (OSO) satellite (1962 ζ) contains an X-ray spectrometer to perform one of its experiments. Three mechanisms were designed for possible use in providing this instrument's scanning function, i.e., for moving the detector along the focal curve. An initial design requirement imposed on one of these mechanisms was that it maintain the moving detector perpendicular to the radiation beam incident from the grating (Figure 1). An engineering model of this scanning mechanism was designed and fabricated.

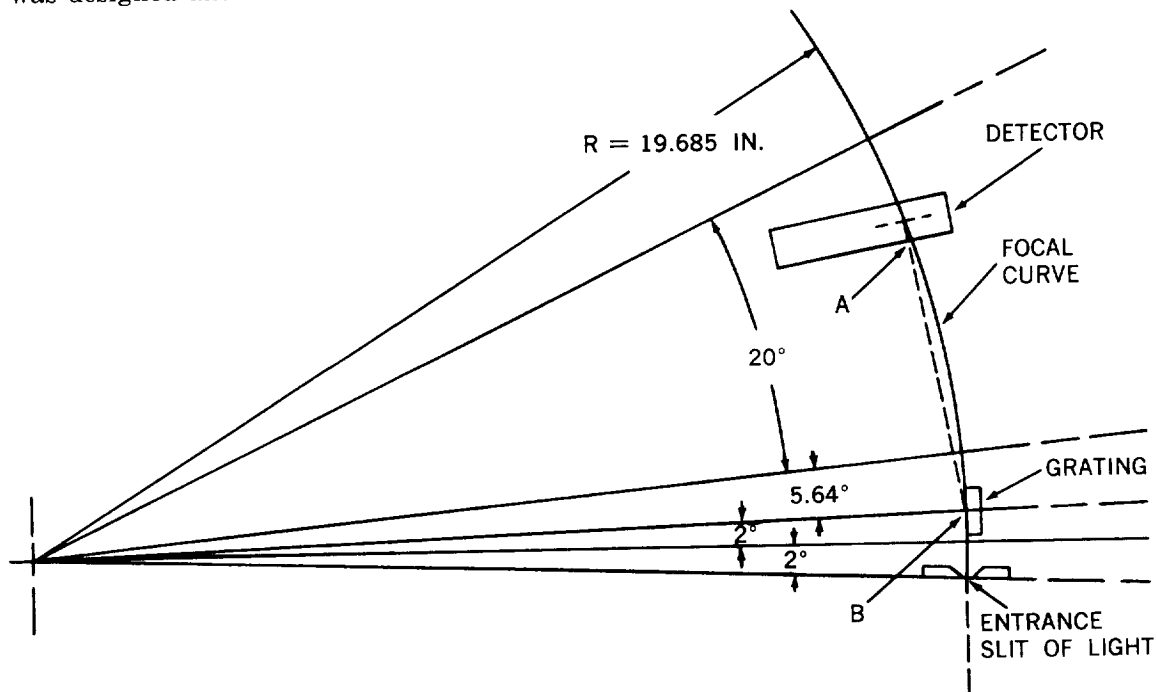


Figure 1 — Layout of detector motion. The incident light from B is perpendicular to the face of the detector at A at all points on focal curve.

The operation of this mechanism may be briefly described as follows: A 6-volt dc motor rotates a drive screw, transmitting linear motion to a main transport carriage through a follower stud mounted in a housing on the carriage (Figure 2). The carriage is constrained by roller bearings between a pair of V-shaped rails which are integral parts of the main housing of the mechanism. A cross-carriage, mounted on the bottom of the main transport carriage, is constrained by grooved bearings between a pair of round rails (Figure 3). One end of the top side of the detector is bearing-mounted to this cross-carriage, allowing the detector to pivot. A bearing on the bottom side of the same end is constrained to move in the focal curve cam mounted directly on the base of the main housing. The opposite end of the detector is supported by means of a grooved bearing in a compensating cam on the main transport carriage. This cam causes the detector to maintain a perpendicular attitude to radiation incident from the grating. The grating is mounted on the base of the main housing (Figure 1).

DESIGN SPECIFICATIONS

The planned orbital characteristics of the satellite were such that the scanning mechanism would have been required to function on a 50 percent duty cycle, i.e., to operate for 40 minutes and then be idle for 40 minutes. This cycling was to continue for 6 months. During the 40-minute "on" period, the detector was to make four

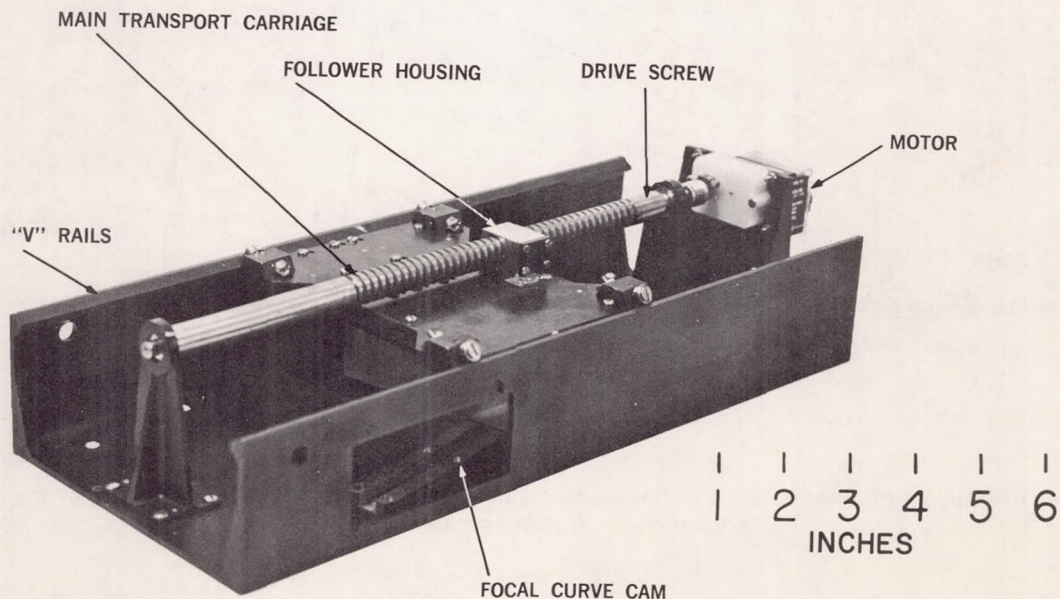


Figure 2 - Photograph of the scanning mechanism

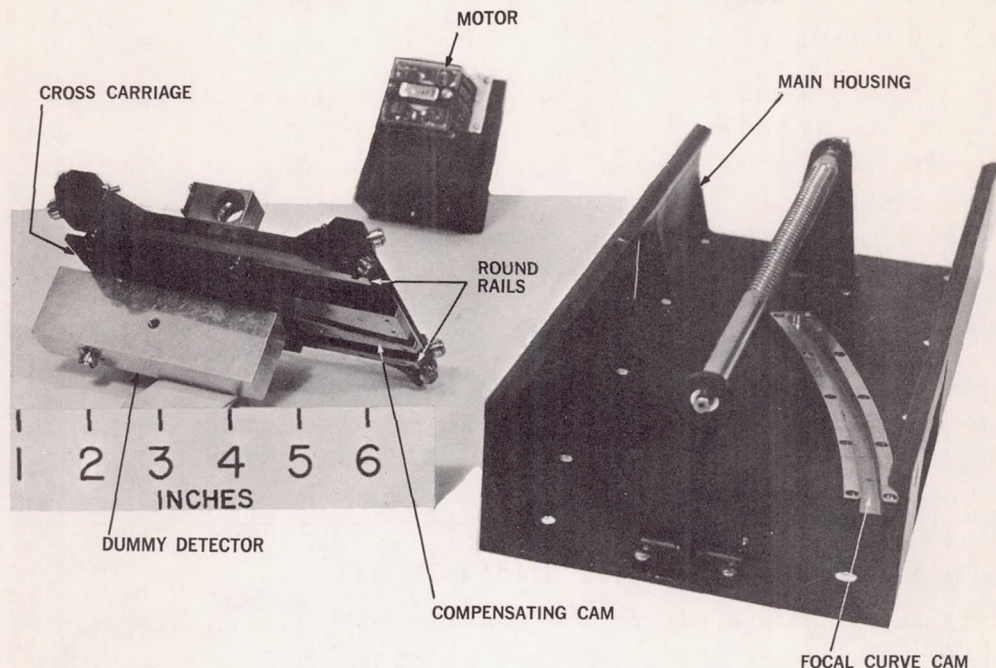


Figure 3 – Photograph of the individual components of the scanning mechanism

scanning passes (two round trips) on the focal curve, each scan requiring 10 minutes. The operating power was not to exceed $\frac{1}{4}$ watt.

The focal curve had a radius of 19.685 inches ($\frac{1}{2}$ meter) and the total angle of travel on the curve was 20 degrees of arc. While scanning the focal curve the detector was to maintain a perpendicular attitude to the beam of radiation incident from the grating. The center of the grating was located at a point on the focal curve, at a distance of 5.64 degrees of arc from the point of closest approach of the detector (Figure 1). The slit through which radiation was directed to the grating was a maximum of 0.787 inch (20 mm) long and was positioned on the same curve, 4 degrees of arc from the center of the grating (9.64 degrees from the closest approach of the detector).

Initially, the exact dimensions of the detector to be used had not been decided. In order to proceed with the design, the dimensions were selected as $3.875 \times 0.780 \times 1.250$ inches. (A dummy aluminum detector was used on the engineering model.) The point on the detector which was to follow the focal curve was located 0.937 inch in from the 1.250-inch edge of the face measuring 1.250×3.875 inches. The dimensions of the grating were $0.984 \times 1.181 \times 0.354$ inch ($25 \times 30 \times 9$ mm). No absolute weight restrictions were placed on the mechanism, but minimal weight was of course desirable. Table 1 lists the weights of the component parts in the experimental mechanism.

The mechanism was required to withstand sinusoidal vibration tests as high as $1\frac{1}{2}$ times the anticipated flight levels, during which it was not required to be operational. It was, however, required to operate properly in the expected orbital temperatures and pressures, ranging from 0° to 50°C and an average of about 10^{-10} mm Hg, respectively.

Table 1
Weight Breakdown of Component Weights in the Experimental
Scanning Mechanism

<i>Linear Moving Parts:</i>	
Carriage, rails, bearings, screws, and pins	272.3 gm.
Compensating cam, screws, and pins	78.3
Undercarriage, bearings, and screws	54.4
Dummy detector	166.9
Reversing stud housing assembly	30.0
	Subtotal 601.9 gm.
<i>Drive Screw</i>	245.5
<i>Remaining Weight</i>	1,028.2
TOTAL WEIGHT	1,875.6 gm. (4.13 lb)

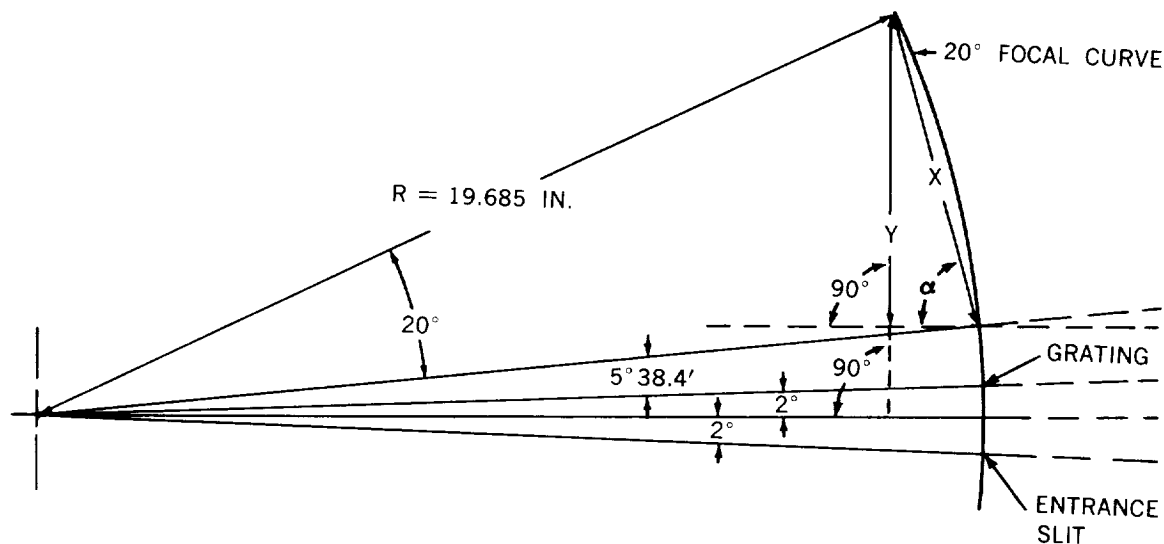
DESIGN, FABRICATION, AND INSPECTION

It was desired that the detector scan the focal curve in both directions without the necessity of reversing the rotation of the driving motor. Two types of drive systems meet this requirement: one based on a chain and sprocket, and the other on a level-wind type of screw. The level-wind screw drive was selected from the standpoint of its relative resistance to the transmission of forces back into the driving-motor mechanism. Besides this, it is relatively simple and trouble-free, should be rugged enough to meet the severe vibration requirements, and is probably the best approach in regard to the severe vacuum-operation requirement.

The most promising motor for powering the drive screw was the Brailsford TR-41M transistorized, brushless, 6-volt dc motor. Limited thermal vacuum tests under a zero load condition had been conducted and the results were encouraging. The speed of the motor was 2800 rpm, reduced to 4 rpm at the output shaft by a self-contained gear reduction unit. Before this motor will meet the final design requirements some design modifications are required; but the motor was adequate for initial testing.

The location of the grating relative to the entrance slit (Figure 4) was such that the most desirable orientation of the drive screw was 90 degrees to the line bisecting the 4-degree angle between the grating and the light entrance slit. With this orientation the effective thread length required on the drive screw was 6.516 inches. At 4 rpm and a scanning time of 10 minutes, a pitch of 0.163 inch/revolution was required.

The formulas for defining the profile of the compensating cam are given in Figure 5 and the resulting cam data in Figure 6. (The value of $A = 26^\circ 8.4'$ is the sum of the 20° focal curve, the $5^\circ 38.4'$ arc, and $1/2^\circ$ for overtravel. The values of angle B were arrived at by arbitrarily dividing the focal curve into eleven equal angles with the vertex at the grating.) The cross section of the compensating cam is in the shape of a square "C". The purpose of making it in this form was to allow the groove bearings, while moving in the cam, to be used to support the detector. The focal curve cam has the shape of an open channel machined to the curvature of the focal curve.



$$\alpha = 80^\circ - (5^\circ 38.4' + 2^\circ) = 72^\circ 21.6'; \quad X = R \frac{\sin 20^\circ}{\sin 80^\circ}$$

$$\text{Thread length } Y = X \sin \alpha = 6.516 \text{ inches.}$$

$$\text{Linear pitch } P = \frac{Y}{4 \frac{\text{rev}}{\text{min}} \times 10 \text{ min}} = 0.163 \text{ inch/revolution.}$$

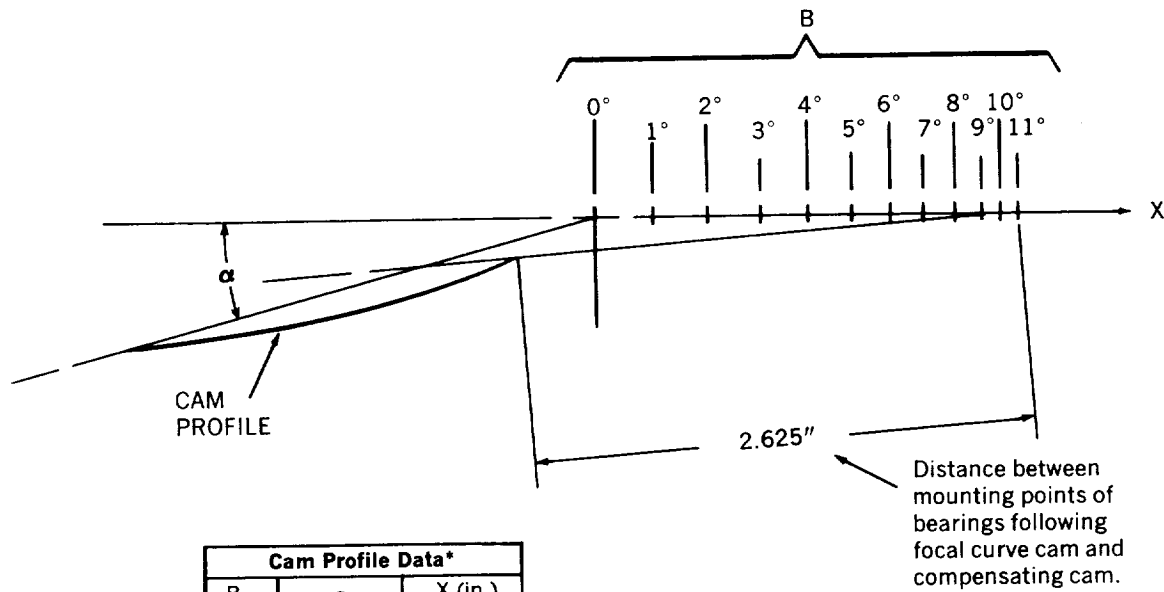
Figure 4 – Thread length and linear pitch on drive screw

After the complete unit was assembled, it was desirable to determine the resulting perpendicular pointing accuracy of the detector. This was accomplished by making measurements on the detector as the drive screw was rotated. The design of the spectrometer was such that only certain dimensions could be measured. The required measurements and formulas, as well as the calculated accuracy, are presented in Appendix A. The pointing angle was calculated as $90^\circ \pm 40'$.

TESTING

The prototype mechanism was tested to as high as the sinusoidal vibration levels listed in Table 2, which were $1\frac{1}{2}$ times the levels actually expected during the period of rocket powered flight. The mechanism was not required to be operational during that period.

A dimensional inspection of the assembled unit, to check the pointing accuracy of the detector, was made before and after each vibration test. The accuracy of $\pm 40'$ remained essentially unchanged. A measurement of the torque required to operate the unit was made: Between the ends of the drive screw the torque was 0.5 to 1.5 in.-oz; at the ends (where the detector reverses direction) it measured 3.0 to 6.0 in.-oz. The output torque of the motor was 11.5 to 13.5 in.-oz. On the first run of the unit, an average cycle time of 13 minutes was observed, with a 15 ma average starting current and an 8.5 ma average running current.



Cam Profile Data*		
B	α	X (in.)
0°	$15^\circ 4.2'$	0
1°	$14^\circ 4.2'$	0.315
2°	$13^\circ 4.2'$	0.610
3°	$12^\circ 4.2'$	0.866
4°	$11^\circ 4.2'$	1.122
5°	$10^\circ 4.2'$	1.339
6°	$9^\circ 4.2'$	1.555
7°	$8^\circ 4.2'$	1.732
8°	$7^\circ 4.2'$	1.890
9°	$6^\circ 4.2'$	2.008
10°	$5^\circ 4.2'$	2.126
11°	$4^\circ 4.2'$	2.205

*See Figure 5 for nomenclature

Figure 6 - Compensating cam profile data

After the preceding tests the unit was completely ultrasonically cleaned, and then placed in a vacuum chamber for further testing. The unit operated continuously for 60 minutes in a vacuum of 5×10^{-5} mm Hg, after which it stopped running. Inspection revealed that the failure was due to misalignment of the detector bearings and to rough spots on the drive screw. When these defects were corrected, the unit was placed in the vacuum chamber for another test. After 10 minutes of operation the unit again stalled. This time the failure was due to binding of the motor-output shaft to the gear box housing. This condition was corrected, but after 20 minutes of operation in a third test, a failure again occurred in the motor gear-box. The reduction gears were sticking to the gear shafts.

At this point it was decided that several refinements should be made on the existing design of the gear reduction unit. An order for new motors was placed.

In the meantime, the scanner was subjected to vibration tests. After successfully passing the two lateral vibration test levels (Table 2), the scanner was vibrated in the thrust direction (perpendicular to the drive screw). Instead of using the thrust vibration levels specified previously (Table 2), new levels were defined by adjusting the input levels, at various frequency ranges, to simulate amplifications believed to have occurred in previous payload tests. These new levels are listed in Table 3.

Table 3
Revised Sinusoidal Vibration Levels Used for Scanner
Vibration Tests in the Thrust Direction

Frequency (cps)	Acceleration (g)	Duration (seconds)
5-28	3.0	86
28-46	4.7	25
46-70	40.0	21
70-120	26.4	27
120-500	10.5	71
500-1000	21.0	35
1000-1400	37.4	17
1400-2000	21.0	17.5

Failure occurred in the 70 cps range at 40 g during the last 2 seconds at this level. The vibration test was stopped. Inspection, while the device was still mounted to the vibration table, revealed that the two cam bearings on the detector were damaged (the outer races cracked and fell off). The vertical rail supports were deformed and they had misaligned the rails; this resulted in looseness of the carriage assembly. Inspection of the disassembled unit revealed roughness in the lower carriage bearings, a damaged detector pivot bearing, and peening of the rails and cams at the bearing points. From all indications it was apparent that most of the damage was started by the deformation of the rails. After the test it was discovered that the amplification factors used in adjusting the vibration levels were far in excess of those actually experienced in previous payload tests—an error that came about in the process of reducing original vibration data. It was decided that the levels listed in Table 2 would be used in future tests, since they gave more correct values of amplification.

Before conducting additional vibration tests, it was necessary to overhaul the damaged mechanism. All bearings, as well as the other damaged parts, were replaced. The main housing was replaced with one having thicker side rail supports (changed from 0.094 to 0.125 in.). Also, the locations of the screws holding the mechanism to the vibration fixture were brought closer to the vertical rails to lessen vibration within the rails.

After the mechanism was rebuilt and dimensionally inspected, vibration tests were

conducted in accordance with the levels specified in Table 2. The unit received no damage during these tests.

Additional vacuum-operation tests were then run. Prior to these tests a very fine gold powder was burnished onto the drive screw and follower stud.* With the 6-volt dc input, the motor required an average 8 ma current, indicating low friction between the drive screw and follower. The unit ran in the vacuum chamber at 5×10^{-5} mm Hg for 96 continuous hours before stopping. Galling in the gear reduction unit was again the cause of failure.

CONCLUSIONS AND RECOMMENDATIONS

The scanning mechanism successfully performed the perpendicular scanning function of the detector as it traversed the focal curve. If it were driven by a motor and gear reduction unit with good vacuum operation characteristics, its usefulness would be greatly increased. A more thorough environmental test program on this mechanism is required before it will be acceptable for use. To render the device suitable for satellite application, the following are recommended:

1. An improved vibration-resistant bearing design incorporating dry-film lubrication techniques;
2. Design improvements on the motor and the gear reduction unit;
3. A lighter weight drive screw;
4. A method of caging the detector during flight vibration, in order to minimize detector vibration.

* This was done because of the good friction characteristics obtained in the bearings of the electric field meter of the Explorer VIII satellite: a 10-micron gold plating had been put on the balls and raceways.

Appendix A

Determination of the Pointing Accuracy

It was necessary to measure the lettered dimensions shown in Figure A1 to calculate the pointing accuracy of the detector from rotation 0 to rotation 40. (The drive screw rotated 40 times.) Table A1 gives measured values for A, B, and C (or α), which were the only dimensions accessible.

Table A1
Measurements Made for Calculation
of the Pointing Accuracy

Rotations of Drive Screw From Point "0"	Measured Dimensions (inches)			Angle α
	A	B	C	
0	6.151	2.355	10.605	—
2	6.107	2.642	10.276	—
4	6.053	2.939	9.942	—
6	5.994	3.233	*	6°25'
8	5.927	3.533	*	6°50'
10	5.854	3.834	*	7°20'
12	5.775	4.133	*	7°55'
14	5.690	4.434	*	8°30'
16	5.601	4.734	7.933	—
18	5.504	5.035	7.601	—
20	5.393	5.338	7.267	—
22	5.291	5.638	6.926	—
24	5.174	5.938	6.600	—
26	5.054	6.238	6.266	—
28	4.924	6.538	5.932	—
30	4.788	6.838	5.600	—
32	4.646	7.136	5.255	—
34	4.494	7.436	4.931	—
36	4.336	7.737	4.597	—
38	4.173	8.036	4.267	—
40	3.997	8.335	3.931	—

* Could not be measured with standard measuring instruments. Angle α was accessible in this area and was measured.

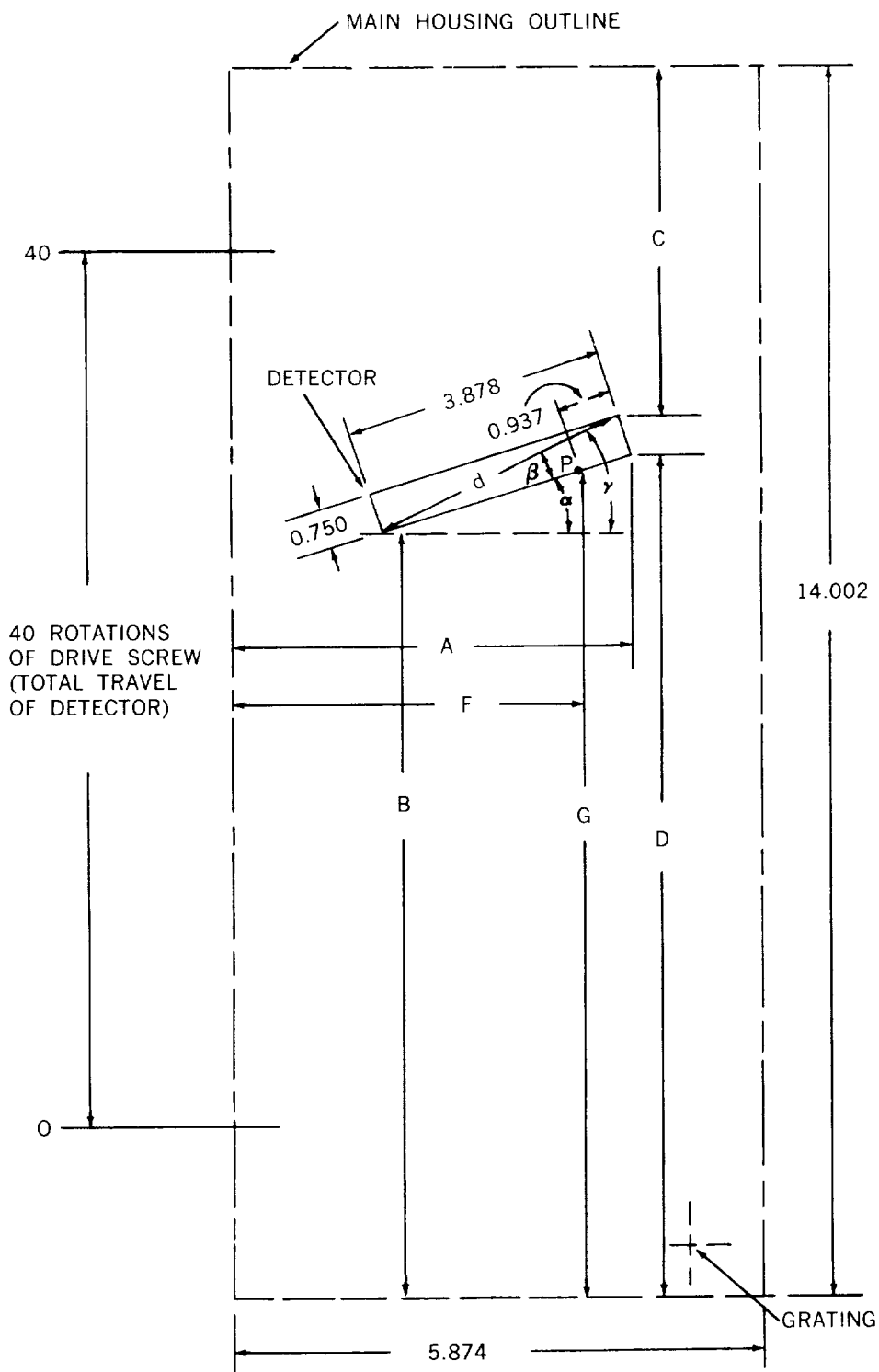


Figure A1 – Dimensions used in determining the pointing accuracy

From the following equations and the values listed in Table A1, the calculated values listed in Table A2 can be derived.

$$\begin{aligned} \sin \gamma &= \frac{14.002 - (B + C)}{d} \\ &= \frac{14.002 - (B + C)}{\frac{0.750}{\sin \beta}} \\ &= \frac{14.002 - (B + C)}{\frac{0.750}{\sin \left[\tan^{-1} \left(\frac{0.750}{3.878} \right) \right]}} ; \\ \gamma &= \sin^{-1} \left[\frac{14.002 - (B + C)}{3.950} \right] ; \\ \alpha &= \gamma - \beta \\ &= \gamma - \tan^{-1} \left(\frac{0.750}{3.878} \right) \\ &= \sin^{-1} \left[\frac{14.002 - (B + C)}{3.950} \right] - 10^{\circ}58' ; \\ \sin \alpha &= \frac{D - B}{3.878} ; \\ D &= B + 3.878 \sin \alpha ; \\ \sin \alpha &= \frac{D - G}{0.937} ; \\ G &= D - 0.937 \sin \alpha ; \\ \cos \alpha &= \frac{A - F}{0.937} ; \\ F &= A - 0.937 \cos \alpha . \end{aligned}$$

Table A2
Calculated Values for Determining the
Pointing Accuracy

Rotations of Drive Screw From Point "0"	α	D	G	F
0	4°20'	2.648	2.577	5.217
2	4°57'	2.977	2.896	5.173
4	5°31'	3.312	3.221	5.120
6	*6°25'	3.667	3.562	5.063
8	*6°50'	3.994	3.882	4.997
10	*7°20'	4.329	4.209	4.925
12	*7°55'	4.667	4.538	4.847
14	*8°30'	5.007	4.868	4.763
16	8°47'	5.326	5.183	4.675
18	9°16'	5.659	5.508	4.579
20	9°45'	5.995	5.836	4.469
22	10°23'	6.337	6.168	4.369
24	10°47'	6.664	6.489	4.254
26	11°19'	6.999	6.815	4.135
28	11°51'	7.335	7.142	4.007
30	12°21'	7.668	7.468	3.873
32	13°6'	8.015	7.803	3.733
34	13°29'	8.340	8.121	3.583
36	14°1'	8.676	8.449	3.427
38	14°31'	9.008	8.773	3.230
40	15°6'	9.345	9.101	3.092

* Corresponding to measured values listed in Table A1.

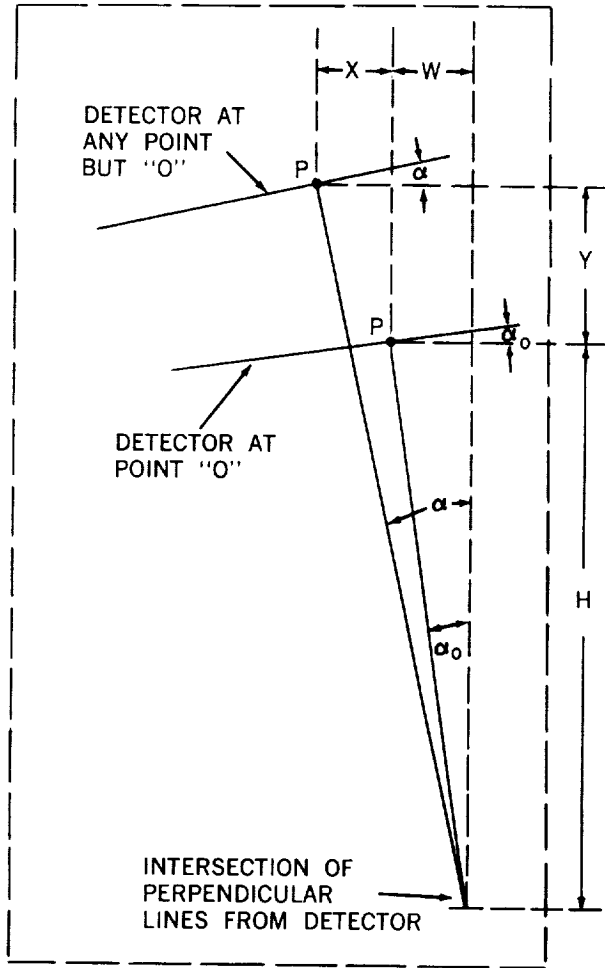


Figure A2 - Pointing accuracy

For incident light to be perpendicular to the detector at P, $\tan \alpha$ must equal $(W + X)/(H + Y)$ where H and W are constants. Also, $\tan \alpha_0 = W/H$ and thus

$$H = \frac{X - Y \tan \alpha}{\tan \alpha - \tan \alpha_0} \quad (\alpha \neq \alpha_0)$$

and

$$W = -X + (H + Y) \tan \alpha .$$

Calculated values of H and W show that they are not constants; therefore the incident light is not perpendicular to P at all times.

We can calculate the variation of the perpendicularity through the use of the maximum and minimum values of H and W. Calculations with these values indicate that the pointing angle is $90^\circ \pm 40'$ for all positions of the detector.



